Synthesis of band and model Hamiltonian theory for hybridizing cerium systems

John M. Wills and Bernard R. Cooper
Department of Physics, West Virginia University, Morgantown, West Virginia 26506
(Received 27 October 1986)

The unusual magnetic behavior of the heavier Ce monopnictides may be understood on the basis of a model Hamiltonian for a system of moderately delocalized f states hybridizing with band states. The parameters entering the theory have previously been taken as phenomenological input. We present a first-principles calculation of the parameters in the model Hamiltonian based on self-consistent, warped-muffin-tin, linear muffin-tin-orbital (LMTO) band structures calculated for CeBi, CeSb, CeAs, and CeP. With the self-consistent potential, we calculate the bands and the band-f hybridization matrix element entering the Anderson lattice Hamiltonian. The band-f hybridization potential is derived from the $4f_{5/2}$ resonance in the potential surrounding a Ce site; the f-state energy with respect to the band Fermi energy and the f-f correlation energy U are estimated by averaging f-state eigenvalues of f^0, f^1, and f^2 Ce configurations. The result is used to calculate the anomalous crystal-field splitting of the Ce $4f_{5/2}$ manifold predicted by the model Hamiltonian for the Ce monopnictides. Due to the structure of the cubic symmetry group, band-f hybridization has a greater effect on the Γ_8 quartet than on the Γ_7 doublet of the $4f_{5/2}$ manifold, and the reduction of the splitting of the crystal-field levels from that expected on extrapolation from the isostructural heavier rare-earth monopnictides may be understood quantitatively on this basis. Our quantitative results are in good agreement with experimental values. We also calculate the range functions describing the anisotropic magnetic behavior of CeBi and CeSb, in fair agreement with phenomenological parameters fitted to data on those materials.

I. INTRODUCTION

The cerium monopnictides, which form in the rocksalt structure, exhibit interesting magnetic behavior. The heavier Ce monopnictides order in complex magnetic structures characterized by strong anisotropy along a cube edge and have complicated magnetic excitation spectra.[1] The paramagnetic crystal-field splitting of the $4f_{5/2}$ manifold in these compounds is much less than expected from extrapolation from other rare-earth monopnictides.[2] These properties can be understood[1,3] as being characteristic of the transition region between itinerant and localized f-electron behavior that occurs for light rare earths (Ce,Pr,Nd) and light actinides (U,Np,P) in appropriate chemical environments. The key aspect of the electronic behavior giving the unusual magnetic properties is the hybridization (mixing) of the f-electrons with band electrons of non-f atomic parentage. The degree of f-electron localization, and hence the importance of hybridization-mediated effects, is sensitive to chemical environment and varies widely depending on the specific compound or alloy.[3] The qualitative dominance of hybridization-mediated effects on the magnetic behavior is expected to diminish strongly on going to the heavier rare earths or actinides in fixed chemical environment (along the rare earth or actinide row for a given isostructural compound such as a monoantimonide), and this expectation is supported by experimental evidence.[3]

The Schrieffer-Wolff transformation[4] on the Anderson Hamiltonian provides a model Hamiltonian from which the unusual magnetic properties arising from the band-f hybridization may be understood.[1] A characteristic parameter that arises in the theory is[5]

$$\mathcal{J}(k,m,n;k',m',n') \equiv -\tfrac{1}{2}V_{km}V^{*}_{k'm'}\left[\frac{1}{\varepsilon_k - E_m - nU}+\frac{1}{\varepsilon_{k'}-E_{m'}-n'U}\right], \tag{1.1}$$

where V_{km} is the band-f hybridization matrix element in the Anderson Hamiltonian, the ε_k are band energies, U is the intra-atomic correlation energy, and E_m+nU is the energy to add an f electron to a Ce f^n configuration. The diagonal elements (in k,k') of $\mathcal{J}$ describe a hybridization induced shift in the f-state energy levels,[5] which may be regarded as a renormalization of the bare crystal-field levels. Hybridization between band states and the Γ_8 quartet of the $4f_{5/2}$ manifold is stronger than hybridization between band states and the Γ_7 doublet of the manifold. This can be understood quantitatively by considering the structure of the cubic symmetry group as described in Sec. IV A, and our quantitative calculations show that the anomalous crystal-field splitting observed in the Ce monopnictides may be understood on this basis. The off-diagonal elements of $\mathcal{J}$ describe a single-site band-f exchange interaction, and the unusual magnetic ordering and magnetic excitation behavior of the heavier Ce monopnictides has been explained in great detail on the basis of a two-ion exchange interaction derived through second-order perturbation theory on the band-f exchange term.[1]

The parameters entering the theory have previously been taken as phenomenological input. While the success

of the theory in describing the diverse magnetic behavior observed in these materials is evidence that the essential physics of the band-f interaction is contained in the model Hamiltonian, the phenomenological parameters that enter the theory do little to elucidate the origins, in the electronic structure, of the observed behavior and lack predictive power in extending the theory to new systems. It is therefore desirable to obtain an absolute, first-principles prediction of the parameters entering the theory.

In this paper, we present a first-principles calculation of the model parameters for CeBi, CeSb, CeAs, and CeP, based on self-consistent, warped–muffin-tin, linear muffin-tin-orbital (LMTO) band structures calculated for these materials. The first step is the generation of a self-consistent, one-electron potential for each compound, calculated with f states treated as corelike states. With the potential thus obtained, we calculate the (non-f) bands and the band-f hybridization matrix element as a function of band index and wave number with a single-site hybridization potential based on the $4f_{5/2}$ resonance in the potential surrounding a Ce site. The f-state energy and the f-f interaction energy U entering Eq. (1.1) are estimated by averaging f-state eigenvalues obtained from Ce muffin-tin potentials with f-state occupations of 0, 1, and 2 electrons.

In Sec. II we review the application of Schrieffer-Wolff theory to the magnetic structure and paramagnetic crystal-field splitting in the Ce monopnictides. Although the phenomenological development is based on the second-order terms in the transformed Hamiltonian, a detailed calculation of the theoretical parameters requires a consistent application of the theory through fourth order in the band-f interaction to avoid singularities induced by the Schrieffer-Wolff transformation. In the Appendix we give a brief description of the fourth-order terms in the transformed Hamiltonian contributing to the exchange interaction describing the magnetic behavior of Ce systems. In Sec. III, we describe the calculation of the bands, the band-f hybridization matrix element, and the f-state energy and f-f interaction U. The calculated parameters are used to obtain the shift in the crystal-field levels in paramagnetic CeBi, CeSb, CeAs, and CeP predicted by the model Hamiltonian, and to calculate the range functions describing the magnetic structure of CeBi and CeSb. In Sec. IV, the predicted crystal-field level shifts are compared with observed values, and the calculated range parameters are compared with phenomenological parameters fitted for those materials.

II. MODEL HAMILTONIAN

The model Hamiltonian is derived from the Anderson Model for a lattice of Ce ions. The spin-orbit splitting of the Ce f states is on the order 0.3 eV, much larger than the band-f interaction and the f-band widths of the Ce monopnictides, and the $4f_{7/2}$ manifold may be neglected. We write the Anderson Model Hamiltonian for the lattice as

$$\begin{aligned}
&\mathcal{H}_A=\mathcal{H}_0+\mathcal{H}_1 \ , \\
&\mathcal{H}_0=\sum_k \varepsilon_k n_k+\sum_{m,R} E_m n_m(R)+\tfrac{1}{2}U\sum_R \hat{N}(R)[\hat{N}(R)-1] \ , \\
&\mathcal{H}_1=\sum_{k,m,R}[V_{km}(R)c_k^\dagger c_m(R)+V_{km}^*(R)c_m^\dagger(R)c_k] \ ,
\end{aligned} \tag{2.1}$$

where the ε_k and E_m are band and f-state energies, U is the intra-atomic f-f correlation energy, V_{km} is the band-f matrix element of a single-particle (hybridization) potential, and R labels the lattice sites. The total number operator $\hat{N}$ in Eq. (2.1) is given by $\hat{N}(R)=\sum_m n_m(R)$. Schrieffer and Wolff[4] defined a canonical transformation e^S designed to diagonalize $\mathcal{H}_A$ through first order in $\mathcal{H}_1$. With S defined so that $[S,\mathcal{H}_0]=-\mathcal{H}_1$, the Schrieffer-Wolff transformation $e^S\mathcal{H}_A e^{-S}$ on the Anderson Hamiltonian results in a Hamiltonian of second and higher order in $\mathcal{H}_1$. Within an f^1 basis, neglecting terms creating or destroying two f electrons at a single site, the second-order term of the transformed Hamiltonian may be written as[5]

$$\begin{aligned}
&\mathcal{H}_S^{(2)}=\mathcal{H}_0'+\mathcal{H}_{\rm ex}+\mathcal{H}_f \ , \\
&\mathcal{H}_0'\equiv\sum_{R,m,m'}\sum_k c_m^\dagger(R)c_{m'}(R)[(1-n_k)\mathcal{J}(k,m',0;k,m,0)+n_k\mathcal{J}(k,m',1;k,m,1)] \\
&\qquad -\sum_{R,m,k} n_m(R)n_k\left[\sum_{m'}\mathcal{J}(k,m',1;k,m',1)\right] \ , \\
&\mathcal{H}_{\rm ex}\equiv-\sum_{k,k'}{}'\sum_{R,m,m'} c_k^\dagger c_{k'}c_{m'}^\dagger(R)c_m(R)[\mathcal{J}(k,m,0;k',m',0)-\mathcal{J}(k,m,1;k',m',1)]e^{-i(\mathbf{k}-\mathbf{k}')\cdot\mathbf{R}} \ , \\
&\mathcal{H}_f\equiv\sum_{R,R'}{}'\sum_{mm'} c_m^\dagger(R)c_{m'}(R')\sum_k \mathcal{J}(km'1,km1)e^{i\mathbf{k}\cdot(\mathbf{R}-\mathbf{R}')} \ ,
\end{aligned} \tag{2.2}$$

with the exchange parameter $\mathcal{J}$ given by Eq. (1.1). The prime on the summations in Eqs. (2.2) denotes $k\neq k'$ and $R\neq R'$. The net effect of the Schrieffer-Wolff transformation, to second order in $\mathcal{H}_1$, is to replace the band-f interaction term in the Anderson Hamiltonian by a direct scattering term $\mathcal{H}_0'$, an exchange scattering term $\mathcal{H}_{\rm ex}$, and an f-f banding term $\mathcal{H}_f$.

The phenomenological theory developed to describe the

magnetic properties of the Ce monopnictides[1] has been based on a superposition of terms obtained by applying the Schrieffer-Wolff transformation to the Anderson model for an isolated Ce impurity, neglecting terms of higher than second order in $\mathcal{H}_1$. The main difference, in second order, between the phenomenological theory and Schrieffer-Wolff theory applied to the Anderson lattice Hamiltonian is the appearance of the term $\mathcal{H}_f$. In the limit $U \to 0$, $\mathcal{H}_f$ may be used to describe the formation of bands from localized orbitals.[6,7] In the limit $U \to \infty$ appropriate for Ce systems, $\mathcal{H}_f$ couples states differing in energy by U; i.e., the bandwidth is suppressed by a factor of $1/U$. The matrix element of $\mathcal{H}_f$ within an f^1 basis vanishes, and for our purposes, $\mathcal{H}_f$ will contribute, in fourth order in $\mathcal{H}_1$, to the high-energy channel ($f^1 \to f^2 \to f^1$) of the two-ion exchange coupling described below (but not to the low-energy ($f^1 \to f^0 \to f^1$) channel).

In this paper, we are concerned with two consequences of Eq. (2.2) applied to the Ce monopnictides: the deviation of the measured paramagnetic crystal field splittings from values expected from extrapolation from other rare-earth monopnictides and the unusual, anisotropic magnetic ordering and excitation behavior exhibited by CeSb and CeBi. The direct scattering piece in Eq. (2.2) is a shift in the f-state energy levels due to hybridization with band states. For the rocksalt structure Ce monopnictides, H_0' may be regarded as a perturbation on the bare crystal-field levels.[8] Transforming to cubic crystal-field coordinates M diagonalizes $\mathcal{H}_0'$, resulting in a shift in the crystal-field levels given by

$$\Delta E_M = \sum_{\varepsilon_k > E_F} \mathcal{J}(k,M,0;k,M,0) + \sum_{\varepsilon_k < E_F} \mathcal{J}(k,M,1;k,M,1) - \sum_{\varepsilon_k < E_F} \left[\sum_{M'} \mathcal{J}(k,M',1;k,M',1) \right] . \tag{2.3}$$

The first term in Eq. (2.3) is negative, and has the largest magnitude if U is large; the second term is positive with a magnitude reduced by a factor of $\sim 1/U$. The last term in Eq. (2.3) is a uniform lowering of the f levels. In general, hybridization between band states and f states will affect the Γ_8 quartet of the Ce $4f_{5/2}$ manifold more strongly than the Γ_7 doublet of that manifold. (This can be seen from the symmetry structure of the cubic group as discussed in Sec. IV A.) The difference in band-f hybridization between the Γ_7 doublet and the Γ_8 quartet will change the splitting of the bare crystal-field levels; the sign and magnitude of the effect depends on the shape and character of the density of states near the Fermi energy and the proximity of the f-state energies E_f and $E_f + U$ to the Fermi energy. In Sec. IV the relative shift in the $\Gamma_7 - \Gamma_8$ splitting predicted by Eq. (2.3) is evaluated for CeBi, CeSb, CeAs, and CeP. We find that the magnitude of the shift in the crystal-field levels gives a good account of the deviation[2] of the measured splittings from expected values. The effect arises from hybridization with bands throughout the Brillouin zone, rather than being dominated by contributions from band states in the vicinity of the zone center.

The exchange scattering Hamiltonian H_{ex} in Eq. (2.2), treated in second-order perturbation theory on band states, results in an indirect, two-ion exchange interaction between Ce f states, mediated by band states. For Ce ions at lattice sites $\mathbf{R}_1$ and $\mathbf{R}_2$, the two-ion exchange interaction takes the form[9]

$$H(1,2) = -\Sigma_{m_1 m_1'} \Sigma_{m_2 m_2'} E(m_2', m_2; m_1', m_1; \mathbf{R}_2 - \mathbf{R}_1) \times c^\dagger_{m_2'}(2) c_{m_2}(2) c^\dagger_{m_1'}(1) c_{m_1}(1) , \tag{2.4}$$

where the range functions $E(\mathbf{R})$ are given by

$$E(m_2', m_2; m_1'; m_1; \mathbf{R}) = -\Sigma_{\varepsilon_k < E_F} \Sigma_{\varepsilon_{k'} > E_F} \times \frac{[J^{m_2' m_2}(k',k)]^* J^{m_1 m_1'}(k',k)}{\varepsilon_k - \varepsilon_{k'}} \times e^{-i(\mathbf{k}-\mathbf{k}')\cdot\mathbf{R}} , \tag{2.5}$$

with

$$J^{mm'}(k,k') = J(k,m,0;k',m',0) - J(k,m,1;k',m',1) . \tag{2.6}$$

The two-ion exchange interaction, Eq. (2.4), with range functions $E(\mathbf{R})$ treated as phenomenological input, has been shown to give a good account[1] of the magnetic ordering and magnetic excitation behavior found in CeSb and CeBi. When the f states in Eq. (2.4) are quantized with respect to the interionic axis and the bands are symmetric about this axis, magnetic quantum numbers are preserved; i.e., $m_1' = m_2$ and $m_2' = m_1$. Furthermore, with these constraints, it may be shown[1,10] that in the limit of large $|\mathbf{R}|$, those range functions for which $m_1, m_2 = \frac{1}{2}$ (equal by symmetry) dominate the two-ion exchange interaction. The phenomenological description of the magnetic behavior of CeBi and CeSb thus uses a single-range parameter for each neighbor shell, corresponding to transitions involving $m, m' = \frac{1}{2}$ states (quantized along the interionic axis); the anisotropic magnetic structures result from this directional coupling in the cubic crystal environment.

The f-level shift, in Eq. (2.3), is well defined. Inserting Eq. (1.1) into Eq. (2.3), it is evident that the energy differences entering the denominators of J are either between unoccupied band states and $E_f < E_F$ or between occupied band states and $E_f + U > E_F$, and hence there are no singularities. Evaluating the range functions, Eq. (2.5), derived from the second-order Hamiltonian (Eq. (2.2), requires summing over bands both above and below the Fermi energy, and we would have to deal with the poles in the exchange parameter, Eq. (1.1). Giving the f level E_f an infinitesimal width is insufficient; the result may be seen to diverge as $[d(\varepsilon_k - E_f)]^2$, and we have previously[11] evaluated Eq. (2.5) using a finite width parameter derived from the $4f_{5/2}$ resonance width of the potential surrounding a Ce site. This procedure is unnecessary, however. As we indicate in the Appendix, keeping all terms consistently to order $(H_1)^4$ both in the Schrieffer-Wolff transformation and perturbation theory on Eq. (2.2), we find a well-defined two-ion exchange interaction, given by Eq. (2.4) with range parameters given by

$$\mathcal{E}(m_2',m_2;m_1',m_1;\mathbf{R})=-\sum_{k,k'} V_{km_2}V^*_{k'm_2'}V_{k'm_1}V^*_{km_1'}e^{-i(\mathbf{k}-\mathbf{k}')\cdot\mathbf{R}}F(\varepsilon_k,\varepsilon_{k'}) , \tag{2.7}$$

with $F(\varepsilon,\varepsilon')$ defined by

$$\begin{aligned}F(\varepsilon,\varepsilon')=&\Theta(E_F-\varepsilon)\Theta(\varepsilon'-E_F)\left[\left[\frac{1}{\varepsilon'-E_f}-\frac{1}{\varepsilon-E_f-U}\right]^2\frac{1}{\varepsilon-\varepsilon'}+\frac{2}{U}\frac{1}{(\varepsilon-E_f-U)(\varepsilon'-E_f)}\right]\\&+\tfrac{1}{2}\Theta(\varepsilon-E_F)\Theta(\varepsilon'-E_F)\left[\frac{1}{(\varepsilon-E_f)(\varepsilon'-E_f)}\left[\frac{2}{U}+\frac{1}{\varepsilon-E_f}+\frac{1}{\varepsilon'-E_f}\right]\right]\\&+\tfrac{1}{2}\Theta(E_F-\varepsilon)\Theta(E_F-\varepsilon')\left[\frac{1}{(\varepsilon-E_f-U)(\varepsilon'-E_f-U)}\left[\frac{2}{U}-\frac{1}{\varepsilon-E_f-U}-\frac{1}{\varepsilon'-E_f-U}\right]\right]\end{aligned} \tag{2.8}$$

where $\Theta(\varepsilon)$ is a step function. The result is somewhat complicated, but with $E_f<E_F<E_f+U$, well defined and relatively insensitive to the position of the f-levels E_f and E_f+U. In Sec. IV, range functions calculated through use of Eqs. (2.7) and (2.8) are found to be in reasonable agreement with phenomenological parameters fitted to the observed magnetic structures of CeBi and CeSb.

III. THE MODEL PARAMETERS

In this section, a correspondence is established between the model Hamiltonian parameters and our one-electron band structures. The first step is the generation of a self-consistent one-electron potential for the Ce monopnictide being studied. We identify the Ce $4f_{5/2}$ states in the model Hamiltonian with the $l=3$, $j=\frac{5}{2}$ resonance in the local potential surrounding a Ce site, and obtain a normalizable f state by imposing a localization potential on the resonant scattering state. This procedure for obtaining a localized f state is performed at each iteration of the self-consistency process in the band calculation; thus the Ce $4f$ state is treated as a self-consistent core state, rather than as an itinerant state. The crystal potential is calculated by iterating to self-consistency with a single valence electron occupying this corelike f state; hybridization between band states and f states is neglected in this process. After achieving self-consistency, we obtain the band-f hybridization potential for input into the model Hamiltonian as the matrix element of the local Hamiltonian at a Ce site between the localized Ce f state and band states, projecting band-f overlap out of the matrix element to correct for band-f nonorthogonality. The extreme localization of the resonant f state about a Ce site and the form of the tails of the LMTO eigenvectors provide a relatively simple form for the band-f matrix element entering the model Hamiltonian. The two remaining parameters we require are the position of the f level E_f with respect to the Fermi energy and the intra-atomic f-f correlation energy U. We identify E_f as the energy required to place the Ce f electron in a band state at the Fermi energy E_F in the unhybridized band-f system, and E_f+U as the energy to remove a band electron from the Fermi level and create an additional f electron, estimating these energies by averaging f-state eigenvalues for Ce muffin-tin potentials calculated with f-state occupations of 0, 1, and 2 electrons.

A. Potential and band structure

The self-consistent one-electron potential describing the band structure of each Ce monopnictide studied is obtained from a warped–muffin-tin LMTO band structure calculation, i.e., an LMTO calculation in which the potential is spherical (except for a small correction) in nonoverlapping spheres and has unrestricted spatial dependence in the interstitial between spheres. This calculation differs from the more common LMTO-ASA (atomic-sphere approximation) method[12] in several features. The basis functions are muffin-tin orbitals based on nonoverlapping spheres. In the interstitial region, these bases have, in general, a nonzero kinetic energy, which is treated as an additional variational parameter. The electron density and potential in the interstitial region are calculated in reciprocal space by expanding the spherical wave bases in Fourier series. The only shape approximation to the potential is a spherical averaging in nonoverlapping muffin-tin spheres surrounding the Ce and pnictogen sites.

Exchange and correlation are treated in the Hedin-Lundqvist[13] version of the local-density approximation. Core states are included self-consistently. The potential is evaluated at the experimental volume, and the radii of the nonoverlapping muffin-tin spheres are chosen by trial and error to make the potential continuous where spheres touch. Geometrical parameters for the Ce monopnictides are given in Table I.

Since crystal-field effects and the change in these effects by hybridization are an important physical feature of the systems being discussed, the point arises that one might expect charge anisotropy with a corresponding cubic contribution to the potential within the muffin-tin spheres.

TABLE I. Geometrical parameters of the self-consistent LMTO band structure calculations for the Ce monopnictides. a is the lattice parameter and s_{Ce} and s_p are the Ce and pnictogen muffin-tin radii, respectively, in atomic units.

	a (a.u.)	s_{Ce} (a.u.)	s_p (a.u.)
CeBi	12.284	3.133	3.009
CeSb	12.118	3.110	2.949
CeAs	11.490	3.052	2.693
CeP	11.210	3.010	2.595

One can then ask whether it is desirable in principle and significant in practice to include these cubic potential corrections to the spherical potential we use in the present calculations. In fact, the prototype materials of the type we want to treat are CeSb and CeBi. For these materials, both from experiment[2] and from our calculations as described below, the hybridization dressing of the crystal field almost exactly cancels the bare crystal field, and the net crystal-field splitting is small. Thus a spherical potential probably provides a better starting potential for the self-consistency procedure than one using a cubic potential corresponding to the bare crystal field. On the other hand, for materials where such close cancellation does not exist, and probably more significantly for magnetically ordered material (as discussed briefly in the final section, it is probably desirable to have the potential within the spheres reflect the lowered symmetry of the system.

The Ce f electrons are treated as localized states rather than itinerant states in this process. The precise definition of the wave functions of these states is given in Sec. III B below; in essence the f electrons are treated (self-consistently) as core states and are not allowed to hybridize with band states.

The radial basis functions for the (non-f) bands are obtained within the muffin-tin spheres from a scalar relativistic radial equation;[14] spin-orbit coupling is recovered perturbatively and self-consistently. The band structure is split into two energy windows: the semicore Ce $5p$ and pnictogen s bands are calculated with an imaginary LMTO tail parameter κ, with $\kappa^2 \approx -0.6$ Ry, and the Ce valence $6s$, $6p$, and $5d$ states and pnictogen valence p and d states are calculated with a tail parameter $\kappa^2 \sim 0.25$ Ry. To maintain a measure of orthogonality to the Ce $4f$ states, the f components of the band tails in a Ce muffin tin are represented by $5f$ orbitals. Core states are obtained from the Dirac equation for the spherically averaged potential at each site. The bands are evaluated at 60 "special" points[15] in the fcc Brillouin zone and iterated until the potential is converged to within less than 0.1 mRy.

The band structure of CeSb, typical of the Ce monopnictides, is plotted along symmetry lines in Fig. 1. The energy of the resonant, corelike Ce $4f_{5/2}$ state lies about 15 mRy below the Fermi energy in this figure. In Sec. IV, we treat the effects of band-f hybridization within the context of the model Hamiltonian. The bands dominating the hybridization-induced properties are largely derived from pnictogen p states and Ce $5d$ states. For the discussion of the hybridization effects given below, it is instructive to consider the composition and symmetry of the bands at point Γ, shown in Fig. 1. Pnictogen p bands at Γ have $\Gamma_6^{(-)}$ and $\Gamma_8^{(-)}$ symmetry. Ce d bands at Γ are bases for three representations, one with $\Gamma_7^{(+)}$ symmetry and two with $\Gamma_8^{(+)}$ symmetry.

Around Γ, the bands exhibit a fair amount of p-d hybridization. At point Γ, both the $\Gamma_8^{(+)}$ ($j=\frac{3}{2}$) and $\Gamma_7^{(+)}$ ($j=\frac{5}{2}$) d states are below the $\Gamma_8^{(-)}$ p states; the bands coming into Γ from above are d bands, however, and the bands coming into point Γ from below are p states. Four bands cross the Fermi energy between point Γ and point X in Fig. 1. The two crossings closest to point Γ are

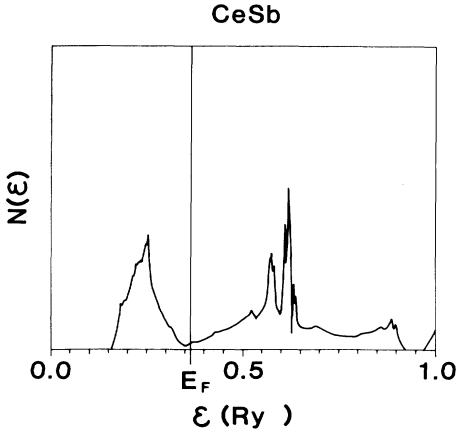

FIG. 2. The density of states of the LMTO band structure of CeSb corresponding to the band structure shown in Fig. 1.

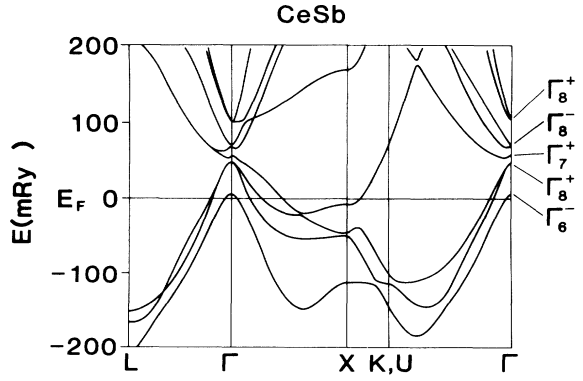

FIG. 1. The warped-muffin-tin LMTO band structure of CeSb, calculated with Ce $4f$ states treated as localized states, without band-f hybridization, along symmetry lines in the fcc Brillouin zone. Energies (in mRy) are measured with respect to the Fermi energy.

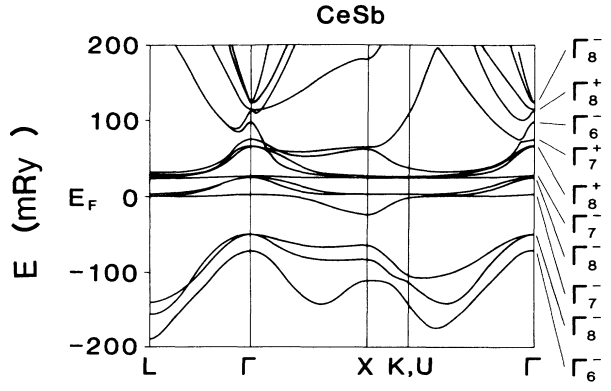

FIG. 3. The warped-muffin-tin LMTO band structure of CeSb, calculated with the Ce $4f$ states treated as band states, along symmetry lines in the fcc Brillouin zone. Energies (in mRy) are with respect to the Fermi energy of the fully hybridized band structure.

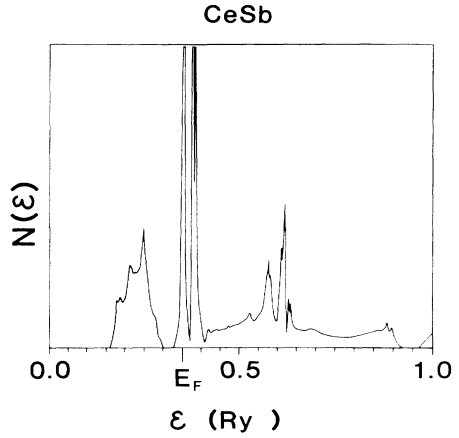

FIG. 4. The density of states of the hybridized band structure of CeSb shown in Fig. 3 (solid line).

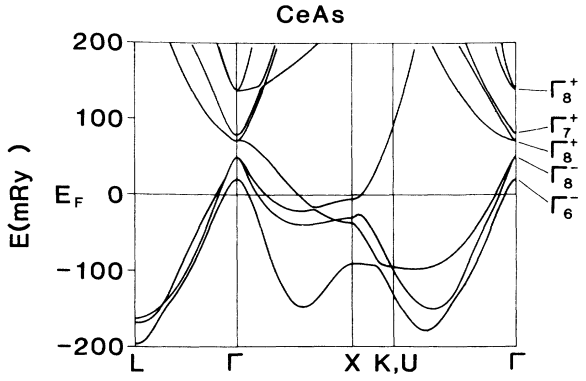

FIG. 6. The band structure of CeAs, calculated with the Ce $4f$ states treated as localized states, along symmetry lines in the Brillouin zone. Energies (in mRy) are with respect to the Fermi energy.

mainly Sb p bands. The two crossings closest to point X are mixed p-d bands; the upper of these two bands has more d character close to point Γ, and more p character close to point X. The density of states corresponding to the band structure in Fig. 1 is given in Fig. 2.

For comparison, Fig. 3 shows the fully hybridized LMTO band structure of CeSb. Ce f states form two sets of flat bands below ($4f_{5/2}$) and above ($4f_{7/2}$) the Fermi energy, hybridizing most strongly with (non-f) band states close to Γ and between Γ and X. At Γ, the $f_{5/2}$ states form two representations ($\Gamma_7^{(-)}$ and $\Gamma_8^{(-)}$ and the $f_{7/2}$ states form three representations ($\Gamma_6^{(-)}$, $\Gamma_7^{(-)}$, and $\Gamma_8^{(-)}$). The density of states corresponding to the band structure of Fig. 3 is given in Fig. 4. The position of the f levels is evident. The center of the $f_{5/2}$ peak (the sharp peak just below the Fermi energy) lies within ~ 1 mRy of the energy of the localized orbital we use to treat the f states in the self-consistency process.

While we will take the energy of the localized orbital ε_f, as characterizing the wave function of the f state entering into hybridization with band states, it is not appropriate to take ε_f as describing the position of the f levels E_f, in the model Hamiltonian. E_f enters the model Hamiltonian as the energy to transfer an f electron to a non-f band state i.e., to change the Ce $4f$-projected charge from 1 to 0 on a single Ce site, and we do not identify ε_f with E_f.

The band structures of CeBi, CeAs, and CeP (calculated with the Ce $4f$ states treated as localized states) are shown in Figs. 5 through 7. The difference in the band structures of the monopnictides (Figs. 1 and 5–7) is accounted for by the decreasing effect of spin-orbit coupling on the pnictogen p bands on going up the pnictogen column: the top of the p-bands (at Γ) falls relative to the bottom of the d bands on passing from the bismuthide to the phosphide.

B. Resonant f state

The wave function representing the Ce $4f_{5/2}$ state is obtained (self-consistently) from the resonance in the potential within a Ce muffin tin. The form we obtain for the band-f hybridization matrix element in the model Hamiltonian follows from this choice, and so we make the

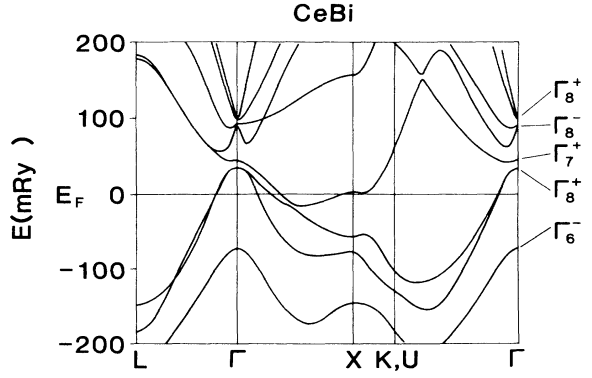

FIG. 5. The band structure of CeBi, calculated with the Ce $4f$ states treated as localized states, along symmetry lines in the Brillouin zone. Energies (in mRy) are with respect to the Fermi energy.

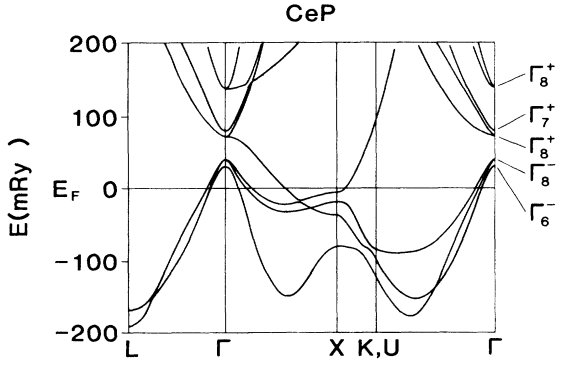

FIG. 7. The band structure of CeP, calculated with the Ce $4f$ states treated as localized states, along symmetry lines in the Brillouin zone. Energies (in mRy) are with respect to the Fermi energy.

definition of this state explicit. The Hamiltonian for an isolated Ce muffin tin, including the spin-orbit interaction explicitly, is defined by

$$\mathcal{H}_{\rm MT}=[-\nabla^2+V_{\rm MT}(r)+V_{\rm s.o.}(r)\sigma\cdot\mathcal{L}]\Theta(s-r)\ ,$$
$$V_{\rm s.o.}(r)=\frac{1}{c^2}\frac{1}{r}\frac{d}{dr}V_{\rm MT}(r)\ , \tag{3.1}$$

where $V_{\rm MT}(r)$ is the self-consistent, spherically averaged potential in a Ce muffin-tin sphere of radius s. This single-site potential has a narrow $f_{5/2}$ resonance with a width of about 3 mRy surrounding the center of gravity of the $4f_{5/2}$ bands in a fully hybridized band structure. The spectral $l=3$ projected density of states for the muffin-tin Hamiltonian $\mathcal{H}_{\rm MT}$ defined by Eq. (3.1) is shown in Fig. 8. The resonant energy, and the resonant radial eigenfunction, $\phi_f(r)$, of $\mathcal{H}_{\rm MT}$ can be defined by[16]

$$\mathcal{H}_{\rm MT}\phi_f(r)\,|\,l,j,m_j\rangle=\kappa^2\phi_f(r)\,|\,l,j,m_j\rangle \tag{3.2a}$$

$$\mathcal{D}[\phi_f(s)]=\mathrm{Re}\{\mathcal{D}[h_3^+(\kappa s)]\} \tag{3.2b}$$

$$\int_0^s dr\,r^2\phi_f(r)^2=1\ . \tag{3.2c}$$

In Eqs. (3.2), $\mathcal{D}$ is the logarithmic derivative functional $\mathcal{D}[f]=sf'/f$ evaluated at the sphere boundary, h_3^+ is the $l=3$ spherical Hankel function of the first kind, and $|\,l,j,m\,\rangle$ is the eigenfunction of total angular momentum with $l=3$ and $j=\frac{5}{2}$. The boundary condition at $r=s$, Eq. (3.2b), corresponds to maximum localization of a spherical wave within the Ce muffin tin. With the normalization given in Eq. (3.2c), $\phi_f(r)$ is, apart from the inclusion of the spin-orbit interaction in the defining potential, identical to an LMTO Ce $4f$ spherical wave basis with tail parameter κ. To obtain a localized (normalizable) function from ϕ_f, we define

$$\psi_f=\frac{1}{\sqrt{N}}\begin{cases}\phi_f(r), & r<s_1 \qquad (3.3a)\\ [\phi_f(s_1)/h_3^+(i\mu s_1)]h_3^+(i\mu r), & r>s_1 \qquad (3.3b)\end{cases}$$

$$\mathcal{D}[\psi_f(s_1)]=\mathcal{D}[h_3^+(i\mu s_1)] \tag{3.3c}$$

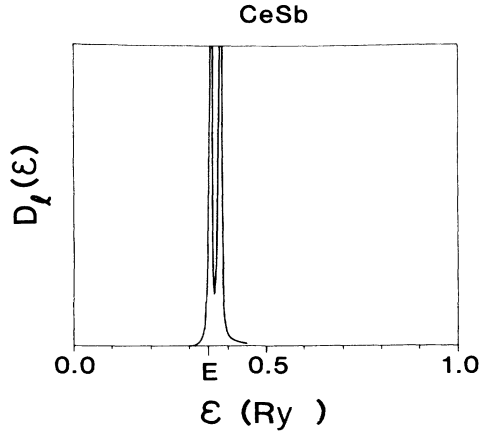

FIG. 8. The spectral weight distribution of the $l=3$ resonance in a Ce muffin-tin potential, defined by $\mathcal{D}_f(\varepsilon)\equiv(1/\pi)\sum_j(2j+1)\partial\delta(l=3,j)/\partial\varepsilon$ where δ is the $4f$ phase shift.

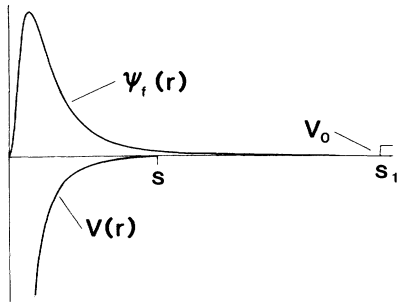

FIG. 9. A schematic of the localized $4f_{5/2}$ radial function ψ_f, defined by Eq. (3.3). $V(r)$ is the self-consistent potential in a Ce muffin tin, referenced to the muffin-tin zero of energy. s is the muffin-tin radius, and s_1 is the radius at which the resonant eigenstate is replaced by exponential decay. V_0 is the effective potential barrier corresponding to the exponential tail of ψ_f. For purposes of display, the magnitude of V_0 is scaled by a factor of 100 relative to $V(r)$.

$$N=\int_0^{s_1}dr\,r^2\phi_f(r)^2+[\phi_f(s_1)/h_3^+(i\mu s_1)]^2\times\int_{s_1}^{\infty}dr\,r^2[h_3^+(i\mu r)]^2 \tag{3.3d}$$

The localization radius s_1 may be chosen within a limited range. The lower limit is set by the condition $\mathcal{D}[\phi_f(s_1)]\le-4(\mu\to0)$, and the upper limit is set by the condition $\phi_f(s_1)\ge0(\mu\to\infty)$. All of the quantities we calculate are insensitive to the choice of s_1, and in practice the localization radius is chosen by requiring that $\mu=\kappa$. The integral of ψ_f^2 over the region $r>s$ is approximately 0.02 for all choices of s_1.

ψ_f is a corelike orbital defined by the Hamiltonian $\mathcal{H}_{\rm loc}=\mathcal{H}_{\rm MT}+V_0\Theta(r-s_1)$, with $V_0=\kappa^2+\mu^2$. Schematic plots of ψ_f and the potential for $\mathcal{H}_{\rm loc}$ are given in Fig. 9. The expectation value of $\mathcal{H}_{\rm MT}$ for ψ_f is

$$\langle\psi_f\,|\,H_{\rm MT}\,|\,\psi_f\rangle=\kappa^2-\delta\kappa^2\ ,$$
$$\delta\kappa^2\equiv(\kappa^2+\mu^2)\int_{s_1}^{\infty}dr\,r^2\psi_f(r)^2\ . \tag{3.4}$$

The energy of the resonant state ϕ_f is lowered an amount $\delta\kappa^2$ by imposing the localization barrier to obtain ψ_f. For all choices of s_1 we find that $\delta\kappa^2/\kappa^2\lesssim0.005$, and ϕ_f is essentially identical to ψ_f.

C. The bands

In the self-consistency process, the band structures are calculated with a tail parameter (for the higher energy window) obtained from an average, over occupied states, of the energy in the interstitial region. To calculate the quantities entering the model Hamiltonian, we require a good representation of the bands around the resonant f-state energy κ^2. Hence the bands entering the model Hamiltonian are obtained, after the self-consistency process, from a final calculation with the energy of the tails of the LMTO bases equal to κ^2.

The hybridization matrix element in the model Hamiltonian will be taken to be the matrix element of $\mathcal{H}_{\mathrm{MT}}$ (Eq. 3.1) between band states and ψ_f. For simplicity, to calculate the hybridization we represent the $f_{5/2}$ component of the nth band at wave-vector $\mathbf{k}$ expanded in spherical waves about a Ce site at $\mathbf{R}=\mathbf{0}$ in the unaugmented form

$$\begin{aligned}&\langle 3,\tfrac{5}{2},m_j \mid \psi^{(n)}(\mathbf{k},\mathbf{r})\rangle_{\mathrm{Ce}}=j_3(\kappa r)\mathcal{T}^{(n)}_{m_j}(\mathbf{k}) ,\\ &\mathcal{T}^{(n)}_{m_j}(\mathbf{k})\equiv\sum_{m_l,m_s}\sum_{\tau,l',m_{l'}}\langle 3,\tfrac{5}{2},m_j \mid 3,m_l,m_s\rangle\mathcal{B}(\kappa,\mathbf{k};\mathrm{Ce}\,3\,m_l;\tau,l',m_{l'})\mathcal{A}^{(n)}_{\tau l' m_{l'} m_s}(\mathbf{k}) ,\end{aligned} \tag{3.5}$$

where j_3 is the $l=3$ spherical Bessel function, $\mathcal{B}$ is proportional to the KKR structure function matrix, and $\mathcal{A}$ is the LMTO eigenvector for the nth band at wave vector $\mathbf{k}$. The product $\mathcal{B}\mathcal{A}$ is summed over sites τ and orbital quantum numbers $(l',m_{l'})$. In the form of Eq. (3.5), the part of the $l=3$ components of the spherical wave bases expanded about a Ce site coming from other sites are represented in their unaugmented form; i.e., without replacing the spherical Bessel function by a linear combination of a solution to the radial wave equation and its energy derivative to obtain orthogonality to core states. To be consistent, we should calculate the non-f band structure with the same expansion in the Ce sphere as is represented in Eq. (3.5). The non-f bands are well converged in the Ce muffin tin for $l\leq 2$, however, and, without band-f hybridization, the $l=3$ component has a negligible effect on these bands. For simplicity, we use the form given in Eq. (3.5) to represent hybridization with the f state, though we calculate the non-f bands as stated above.

D. Band-f hybridization

The model Hamiltonian parameter V_{km} is a matrix element of the Hamiltonian for a single-particle potential surrounding a Ce site between band states and the Ce $4f_{5/2}$ state. With band states given by Eq. (3.5), it is evident that the matrix element of a spherically symmetric mixing Hamiltonian between band states and ψ_f will have the form

$$V_{n\mathbf{k},m}=\langle j_3 \mid \mathcal{H} \mid \psi_f\rangle[\mathcal{T}^{(n)}_m(\mathbf{k})]^* . \tag{3.6}$$

We consider the Hamiltonian entering the radial matrix element in Eq. (3.6) to be the idealized, single-site muffin tin Hamiltonian $\mathcal{H}_{\mathrm{MT}}$ defined by Eq. (3.1). The band states as defined by Eq. (3.5) are not orthogonal to ψ_f, and we should project band-f overlap out of the matrix element.

We thus define a hybridization potential $v(\kappa)$ through

$$\begin{aligned}v(\kappa)&\equiv\frac{1}{\sqrt{\Omega}}\langle j_3 \mid (1-\mid\psi_f\rangle\langle\psi_f\mid)\mathcal{H}_{\mathrm{MT}}\mid\psi_f\rangle\\ &=\frac{1}{\sqrt{\Omega}}\{\langle j_3\mid V\mid\psi_f\rangle+[\langle j_3\mid-\nabla^2\mid\psi_f\rangle-(\kappa^2-\delta\kappa^2)\langle j_3\mid\psi_f\rangle]\}\\ &=\frac{1}{\sqrt{\Omega}}\left[\int_0^s dr\,r^2 j_3(\kappa r)[V_{\mathrm{MT}}(r)-4V_{\mathrm{s.o.}}(r)]\psi_f(r)+\delta\kappa^2\int_0^\infty dr\,r^2 j_3(\kappa r)\psi_f(r)\right] ,\end{aligned} \tag{3.7}$$

where the energy shift $\delta\kappa^2$ is given in Eq. (3.4). The factor of the square root of the unit cell volume, Ω, has been included in Eq. (3.7) to give $v(\kappa)$ the units of a potential. Projecting band-f overlap out of the matrix element cancels the kinetic energy contribution within the Ce sphere, leaving a residual contribution proportional to the localization induced shift in the resonant energy κ^2. The first term on the right hand side of Eq. (3.7) is related to $\delta(l=3,j=\frac{5}{2})$, the $l=3$, $j=\frac{5}{2}$ phase shift. With the normalization of ϕ_f given in Eq. (3.2c),

$$\sin[\delta(l=3,\,j=\tfrac{5}{2})]=\left[\frac{\Gamma}{2\kappa N}\right]^{-1/2}\int_0^s dr\,r^2 j_3(\kappa r)(V_{\mathrm{MT}}-4V_{\mathrm{s.o.}})\psi_f(r) , \tag{3.8}$$

where Γ is the width of the Ce $4f_{5/2}$ resonance. The $l=3$ potential scattering[16] is negligible, and we may take $\sin(\delta)\approx 1$. The first term on the right hand side of Eq. (3.7) is thus equal to $-(\Gamma/2\kappa)^{1/2}$. The second term on the right hand side of Eq. (3.7) can be calculated analytically with the exception of the overlap integral for $r<s$, which is readily obtained by numerical integration. The result is insensitive to the choice of localization radius, and we find for all the materials we consider that this term is less than 1% of the magnitude of the first term.

We will thus consider the hybridization potential $v(\kappa)$ to be given by

$$v(\kappa)\approx-\left[\frac{\Gamma}{2\kappa N\Omega}\right]^{1/2} . \tag{3.9}$$

The only dependence on the localizing procedure used to go from ϕ_f to ψ_f left in Eq. (3.9) is the normalization constant. In all cases, $N\lesssim 1.02$, and thus the hybridization potential $v(\kappa)$ is virtually independent of the *ad hoc* procedure we have used to produce an integrable basis function; the hybridization potential is set by choosing the resonant f state to represent f state in the model Hamiltonian. The resonance width is calculated from[16]

TABLE II. Ce $4f_{5/2}$ resonance widths, Γ, and hybridization potentials, $\nu(\kappa)$, in mRy, calculated with Eqs. (3.9) and (3.10), respectively.

	Γ (mRy)	$\nu(\kappa)$ (mRy)
CeBi	4.23	−2.77
CeSb	3.06	−2.41
CeAs	4.28	−2.97
CeP	4.99	−3.25

$$\frac{\Gamma}{2}=\frac{1}{\kappa}\frac{[\phi_f(s)]^2}{|h_3^+(\kappa s)|^2}\ . \tag{3.10}$$

Resonance widths Γ and hybridization potentials ν are given in Table II. Finally, we arrive at the matrix element $V_{n\mathbf{k},m}$, between the nth band at wavevector $\mathbf{k}$ and a Ce $4f_{5/2}$ state with angular momentum quantum number m, as

$$V_{n\mathbf{k},m}=\nu(\kappa)\sqrt{\Omega}[\mathcal{T}_m^{(n)}(\mathbf{k})]^*\ , \tag{3.11}$$

where $\mathcal{T}_m^{(n)}$ is given by Eq. (3.5).

In summary, we have used a self-consistent one-electron warped–muffin-tin potential to define the parameters entering the model Hamiltonian. The f state and the hybridizing Hamiltonian are obtained from the local potential surrounding a Ce site, defined within the confines of the Ce muffin-tin sphere. The bands are obtained from the full crystal potential.

The arbitrariness introduced in the choice of a localization potential for the f state has little effect on the result for $V_{n\mathbf{k},m}$. In the form of Eq. (3.8), the hybridization potential and hence $V_{n\mathbf{k},m}$ is largely independent of this choice and of the behavior in the region outside the Ce sphere which we have neglected. The other quantities entering the calculation (e.g., the resonance energy κ^2) are exactly determined by the self-consistent potential and are not arbitrary parameters.

E. The f-state energy levels

In the model Hamiltonian, the energy difference E_F-E_f is the total energy necessary to place the Ce f electron in a band state at the Fermi energy. Similarly, E_f+U-E_F is the energy required to change from an f^1 to an f^2 configuration. These energies may be obtained from supercell calculations with an f electron removed from or added to a central Ce site.[17] Within the accuracy with which we can expect to calculate the shift in the crystal-field splitting [Eq. (2.3)] and the range functions [Eq. (2.6)], the results are insensitive to shifts in E_f and U of ~ 1 eV, and for our purposes, a more approximate procedure will suffice.

We estimate the character of the screening charge by analyzing the charge density of band structures calculated with 0 or 2 valence electrons placed in the localized orbitals ψ_f. The result is the addition or subtraction of ~ 1 unit of charge of Ce d character.

To estimate E_f and U, we start with the charge density in a Ce muffin-tin sphere calculated with the self-consistent band structure described in Sec. III A. For E_f, using the Ce $l=2$ and $l=3$ radial basis functions, we replace a unit of f charge density by a unit of d charge density, and recalculate the Ce muffin-tin potential and find the $l=3$ resonant energy ε_f^0. Averaging this energy with ε_f, the $l=3$ resonant energy of the self-consistent Ce potential, yields a transition state estimate of $E_F-E_f\approx 2$ eV. Repeating the calculation with the d projected Ce muffin-tin charge replaced by a unit of f charge, yields a transition state estimate of $E_f+U-E_F\approx 4$ eV, which gives a value for U of 6 eV. Calculating E_f and U in this manner gives similar results for all the Ce monopnictides we consider, and in our calculations we use values of $E_f=E_F-2$ eV and $U=6$ eV for all of the Ce monopnictides. This procedure is rather crude, but yields values in reasonable agreement to those reported elsewhere.[17,18]

IV. THE ANOMALOUS CRYSTAL-FIELD SPLITTING AND TWO-ION EXCHANGE COUPLING

In this section, the formalism described in Sec. III is applied to the calculation of the f-level shift, ΔE_M [Eq. (2.3)], in CeBi, CeSb, CeAs, and CeP, which we use to interpret the observed crystal-field splitting of the f-state energy levels, and to the calculation of the range parameters, $\mathcal{E}(\mathbf{R})$ [Eq. (2.5)], for CeBi and CeSb, which are compared with phenomenological parameters describing the magnetic ordering in these materials. The principal parameter in the model Hamiltonian is the exchange coefficient $\mathcal{J}$ [Eq. (1.1)], but it is computationally more efficient to obtain the quantities we desire by first evaluating a second order (in $\mathcal{H}_1$), energy dependent matrix $V(\varepsilon,\mathbf{R})$ connecting Ce f states through hybridization with band states. This is defined by

$$V_{mm'}(\varepsilon,\mathbf{R})\equiv\frac{1}{N(\varepsilon)}\frac{\Omega}{(2\pi)^3}\times\sum_n\int d^3k\ V_{n\mathbf{k},m}^*V_{n\mathbf{k},m'}\delta(\varepsilon-\varepsilon^{(n)}(\mathbf{k}))e^{-i\mathbf{k}\cdot\mathbf{R}} \tag{4.1}$$

from which we may calculate ΔE_M and $\mathcal{E}(\mathbf{R})$. In Eq. (4.1), $\varepsilon^{(n)}(\mathbf{k})$ is the eigenvalue of the nth band at wave vector $\mathbf{k}$, $N(\varepsilon)$ is the density of states, and the matrix elements $V_{n\mathbf{k},m}$ are defined by Eq. (3.11). Ω is the unit cell volume. The bands are evaluated on an 89 point mesh in the irreducible wedge of the fcc Brillouin zone, and integrals over the Brillouin zone are obtained by projecting into and integrating over the irreducible wedge using the tetrahedral scheme of Gilat and Bharatiya.[19]

A. Hybridization-induced anomalous crystal-field splitting

With the exception of Ce, the crystal-field splitting of the ground state multiplet of the rare-earth monopnictides is well described by the crystal field arising from a charge distribution exterior to the region occupied by the f electrons and equivalent to that for a point charge of $-1.2e$ on each nearest-neighbor anion site.[2] Table III compares the measured crystal-field splitting in the Ce monopnictides with values extrapolated from the

TABLE III. The crystal-field splitting in the Ce monopnictides. Δ_{CF} is the difference in energy between the Γ_8 quartet and the Γ_7 doublet (the ground state) of the Ce $4f_{5/2}$ manifold; extrapolated values are values expected on the basis of the point-charge model applied to the other rare-earth monopnictides (Ref. 2), as explained in the text. δE_{CF}, defined by Eqs. (4.2) and (2.3) is the suppression of the crystal-field splitting resulting from band-f hybridization; "measured" values are the difference between extrapolated point-charge values and measured crystal-field splittings. The contributions from Ce d states and pnictogen p states are obtained using densities of state projected onto orthogonalized basis states as explained in the text. All energies are in K.

	CeBi	CeSb	CeAs	CeP
Δ_{CF} (K)				
Measured[a]	8	37	137	150
Extrapolated[b]	247	264	345	390
δE_{CF} (K)				
Measured	239	227	208	240
Calculated				
Total	217	194	195	222
Ce d	172	175	209	243
Pnictogen p	30	5	−26	−36

[a]Reference 19.
[b]Reference 2.

other rare-earth monopnictides. In CeBi and CeSb, the crystal field levels are approximately degenerate, while in CeP and CeAs the measured splitting is about half that expected; the *suppression* of the point-charge crystal-field splitting is approximately constant throughout the pnictogen column, ranging from ~210 K for CeAs to ~240 K for CeP and CeBi.

This behavior may be understood as the result of a shift in the bare crystal-field levels due to the coupling ΔE_M [Eq. (2.3)] between Ce $4f_{5/2}$ states and unoccupied band states. We assume that the unhybridized f levels E_M are those that would be obtained by extrapolation from the heavier rare-earth monopnictides and identify the observed crystal-field levels with $E_M+\Delta E_M$ where ΔE_M is given by Eq. (2.3). The crystal-field splitting $E(\Gamma_8)-E(\Gamma_7)$ will be changed from the extrapolated values by an amount $-\delta E_{CF}$ where

$$\delta E_{CF} \equiv \Delta E(\Gamma_7) - \Delta E(\Gamma_8) \ . \tag{4.2}$$

Comparing Eqs. (1.1), (2.3), and (4.1), we evaluate ΔE_M by use of the formula

$$\Delta E_M = -\sum_{m,m'} \int d\varepsilon \, N(\varepsilon) D^*_{m'M} V_{m'm}(\varepsilon,0) D_{mM} \times \left[\frac{\Theta(\varepsilon - E_F)}{\varepsilon - E_f} + \frac{\Theta(E_F-\varepsilon)}{\varepsilon - E_f - U} \right] , \tag{4.3}$$

where D_{mM} gives the transformation between angular momentum (m) and crystal-field (M) states. The Fermi energy E_F entering Eq. (4.3) is calculated from the band structure without band-f hybridization (shown in Fig. 5). The f-level E_f is placed below E_F as discussed in Sec. III.

The suppression of the bare crystal-field splitting δE_{CF} calculated through the use of Eqs. (4.2) and (4.3), is given in Table III. Agreement with the suppression deduced by comparing observed crystal-field splitting values[20] with extrapolated values is excellent. In general, Eq. (4.3) underestimates the magnitude of the shift by ~20 K (~8%).

The bands which dominate the energy level shift are derived from Ce d states and pnictogen p states. The bands giving rise to ΔE_M may be analyzed by replacing the full density of states $N(\varepsilon)$ in Eq. (4.3) by a projected density of states. A site and angular momentum projection giving the charge decomposition of the bands is indicative of the parentage of the bands, but is misleading except at high-symmetry points. Within our nonorthogonal basis set, there is no unique way to define the decomposition by basis of the bands giving rise to ΔE_M, but we can obtain a reasonable estimate of the parentage of the bands by using a technique of symmetric orthogonalization[21] to project the density of states onto orthogonalized basis states. The relative contributions from Ce $5d$ and pnictogen p projected functional densities are given in Table III. To display the relative contributions to the anomalous crystal-field splitting from Ce d and pnictogen p bands, in Fig. 10 we plot $\partial \delta E^{(n)}_{CF}/\partial\varepsilon$, where $\delta E^{(n)}_{CF}$ is obtained from Eqs. (4.2) and (4.3) using the density of states projected on the nth basis state, for CeSb. We are hesitant to attach too much significance to this labeling of contributions as p or d. A more meaningful result is evident from a comparison of Fig. 10 and the band structures of the Ce monopnictides (Figs. 1 and 5–7). In our analysis, a rather insignificant part of the shift in the crystal-field splitting arises from the hole surface around Γ, or, in general from behavior in the immediate vicinity of any high symmetry point.

Takahashi *et al.*[22] have explained the anomalous crystal-field splitting in CeBi and CeSb as arising from coupling between f states and pnictogen p holes at Γ. Their formula, based on second-order perturbation theory, is similar to Eq. (4.3). They note that pnictogen p-f matrix elements are larger than Ce d-f matrix elements, since the pnictogen-Ce distance is smaller than the Ce-Ce separation, and they point out that, at the Γ point, the pnictogen p states mix exclusively with the Γ_8 quartet,

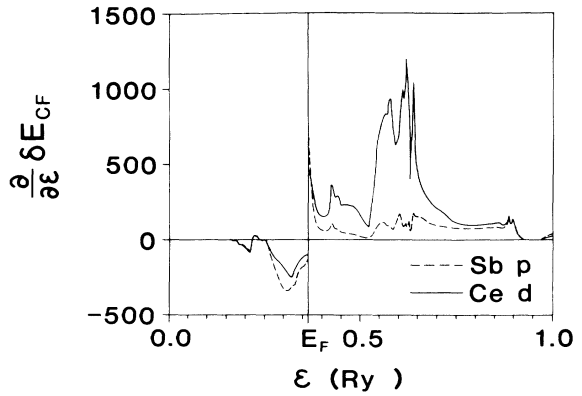

FIG. 10. The contribution to the reduction, δE_{CF} [Eq. (4.2)], in the crystal-field splitting, as a function of energy (in Ry), arising from Sb p states (dashed line) and Ce d states (solid line) in CeSb.

while Ce d states do not hybridize with f states at Γ.

Our quantitative analysis indicates that hybridization between f states and band states throughout the Brillouin zone, rather than just in the vicinity of high-symmetry points, is important to understanding the magnitude of the relative shift in the crystal-field levels. The set of degenerate bands belonging to the star of a general point in the irreducible wedge of the Brillouin zone form a basis for a representation of the cubic group that, like the "regular" representation, contains the Γ_7 representation twice and the Γ_8 representation four times. Hence, with twice the number of states hybridizing with the Ce $4f$ Γ_8 quartet, we expect the effect on the Γ_8 quartet to be larger than the effect on the Γ_7 doublet by approximately a factor of two. Our results confirm this expectation. Both Γ_7 and Γ_8 f states are lowered, with the effect on Γ_8 greater than the effect on Γ_7 by a factor of 2.45 for CeBi, 2.56 for CeSb, 2.16 for CeAs, and 2.09 for CeP. While the coupling between f states and bands at points of high symmetry is strongest and predominantly p-f like, these points, in our analysis, play a limited role in causing the anomalous crystal-field effect. The determining factors are the density of states near the Fermi energy (i.e., arising from band states throughout the Brillouin zone) and the proximity of f-state energy levels to the Fermi energy.

B. Two-ion exchange coupling

CeSb and CeBi order magnetically in a series of complex magnetic structures,[23] characterized by ferromagnetic ⟨001⟩ planes with moments aligned or antialigned along the ⟨001⟩ direction in various stacking arrangements; CeSb also orders in similar structures containing nonmagnetic planes. The magnetic excitation behavior of these materials is anisotropic, showing little dispersion for wavevector parallel to the ⟨001⟩ direction.[24]

This behavior has been explained[1,10,25,26] on the basis of a phenomenological treatment of the two-ion exchange Hamiltonian Eq. (2.4). In this analysis, based on bands of free-electron symmetry,[1] a single parameter suffices to describe the two-ion interaction for each symmetry shell of lattice vectors. As a consequence of the azimuthal symmetry of free-electron bands about any interionic axis $\mathbf{R}$, the angular momentum component along $\mathbf{R}$ ($\mathbf{J}\cdot\mathbf{R}/R$) is conserved by the two-ion interaction [Eq. (2.4)]; hence, in Eq. (2.5), with f-states $|m\rangle$ quantized with respect to $\mathbf{R}$, $m_2=m_1'$ and $m_2'=m_1$. Thus the range function matrix $\mathcal{E}(\mathbf{R})$ may be obtained, through rotations, from a single six-by-six matrix for each neighbor shell. Furthermore, it may be shown[1] that the longitudinal symmetry of free-electron bands about $\mathbf{R}$ implies that, in the limit $k_F R\to\infty$, the only nonzero components of $(k_F R)^3\mathcal{E}(\mathbf{R})$ are those for which $m,m'=\pm\frac{1}{2}$ with respect to $\mathbf{R}$. These components are equal by symmetry; hence a single parameter $\mathcal{E}_n$ determines the range function matrix for each symmetry shell n. The phenomenological two-ion interaction, Eq. (2.4), is thus a directional coupling tending to accumulate charge along the interionic axes;[1,10] when summed over the cubic lattice of Ce ions, the interaction strongly favors a moment aligned along a cube edge,[1,10] reproducing the anisotropic magnetic ordering observed in CeBi and CeSb.

In the phenomenological treatment,[1,10] the range parameters are evaluated by fitting various features of the experimental behavior; e.g., the nearest-neighbor parameter $\mathcal{E}_1$ is fit to the Néel temperature, the ratio $\mathcal{E}_2/\mathcal{E}_1$ is fit to give the observed moment, and $\mathcal{E}_3$ is adjusted to stabilize the magnetic structures at the observed temperatures.[10] Characteristic of the phenomenological parameters for CeBi is that $\mathcal{E}_1$ and $\mathcal{E}_2$ are ferromagnetic with $\mathcal{E}_2/\mathcal{E}_1\gtrsim 1$, and $\mathcal{E}_3$ is antiferromagnetic with $\mathcal{E}_3/\mathcal{E}_1\sim -0.3$.[1,26] Three neighbor shells are generally found to be sufficient to describe the experimental behavior.

The simplicity of the phenomenological range parameters will not be present in range functions calculated with the formalism of Sec. III. With the lower crystal symmetry of the rocksalt structure bands, $\mathbf{J}\cdot\mathbf{R}/R$ is not conserved; furthermore, the symmetries of the matrix $\mathcal{E}(\mathbf{R})$ depend on the particular neighbor shell to which $\mathbf{R}$ belongs. We shall simply compare the appropriate components of $\mathcal{E}(\mathbf{R})$ with the smaller phenomenological matrix. Hence, in what follows, we shall consider only the six-by-six range function matrix given, for a lattice vector $\mathbf{R}$, by

$$\mathcal{E}(m,m';\mathbf{R})\equiv\mathcal{E}(m',m;m,m';\mathbf{R}) , \tag{4.4a}$$

where the axis of quantization is taken along $\mathbf{R}$; e.g.,

$$\frac{\mathbf{J}\cdot\mathbf{R}}{|\mathbf{R}|}|m\rangle=m\,|m\rangle . \tag{4.4b}$$

To calculate $\mathcal{E}(\mathbf{R})$, defined by Eq. (4.4), we first transform $V(\varepsilon,\mathbf{R})$ [Eq. (4.1)] according to

$$V_{mm'}(\varepsilon,\mathbf{R})=\sum_{\mu,\mu'}\mathcal{D}^{(5/2)}_{m\mu}(\mathbf{R})V_{\mu\mu'}(\varepsilon,\mathbf{R})[\mathcal{D}^{(5/2)}_{m'\mu'}(\mathbf{R})]^* , \tag{4.5}$$

where $\mathcal{D}$ is an angular momentum rotation matrix using the convention of Edmonds,[27] and Greek indices refer to f states quantized with respect to the crystal coordinate system. The transformation is unique up to an μ-dependent phase factor, which has no effect on our re-

TABLE IV. Range parameters $\mathcal{E}_n$, defined in Sec. IV B, calculated by use of Eqs. (4.1) and (4.5), compared with phenomenological range parameters fitted to the magnetic structure of CeBi (Ref. 23) as explained in the text.

	CeBi		CeSb
	Fitted[a]	Calculated	Calculated
$\mathcal{E}_1$	14.5 K	0.84 K	0.84 K
$\mathcal{E}_2/\mathcal{E}_1$	1.0	3.33	3.08
$\mathcal{E}_3/\mathcal{E}_1$	−0.3	+0.08	−0.02

[a]Reference 23.

sults. Comparing Eqs. (2.7), (2.8), and (4.1), we obtain $\mathcal{E}(\mathbf{R})$ [Eq. (4.4)] as

$$\mathcal{E}(m,m';\mathbf{R}) = -\int_{-\infty}^{\infty} d\varepsilon \int_{-\infty}^{\infty} d\varepsilon' N(\varepsilon)N(\varepsilon')V_{m'm'}(\varepsilon,\mathbf{R}) \times V^*_{mm}(\varepsilon',\mathbf{R})F(\varepsilon,\varepsilon') , \quad (4.6)$$

where $F(\varepsilon,\varepsilon')$ is given by Eq. (2.8).

To compare the matrix $\mathcal{E}(\mathbf{R})$ calculated through Eq. (4.6) with the phenomenological parameters, one final step is required. $\mathcal{E}(\mathbf{R})$ is not a Hermitian matrix. The phenomenological calculation treats the interaction Hamiltonian [Eq. (2.4)] with mean-field theory; since we are approaching the magnetic ordering from the paramagnetic limit, we should symmetrize $\mathcal{E}(\mathbf{R})$ calculated with Eq. (4.6), and compare $[\mathcal{E}(m',m;\mathbf{R})+\mathcal{E}^*(m,m';\mathbf{R})]/2$ with the phenomenological parameters.

The matrices $\mathcal{E}(\mathbf{R})$ calculated using Eq. (4.5) for CeBi and CeSb reproduce the relative values of the phenomenological parameters, although the magnitudes are smaller, probably indicating a Néel temperature of a few degrees rather than the experimental 16 K for CeSb. We find that those components for which $m,m'=\pm\frac{1}{2}$ dominate the matrix for nearest and next nearest neighbors, by about a factor of two. These components, which we have called $\mathcal{E}_n$, reproduce some of the characteristics of the phenomenological parameters. $\mathcal{E}_1$ and $\mathcal{E}_2$ are ferromagnetic. $\mathcal{E}_3$ is antiferromagnetic for CeSb but ferromagnetic for CeBi; the calculated ratio $\mathcal{E}_3/\mathcal{E}_1$ is much smaller than the phenomenological ratio. The magnitude of $\mathcal{E}_1$ is considerably smaller than the phenomenological $\mathcal{E}_1$ while the ratio $\mathcal{E}_2/\mathcal{E}_1$ is somewhat larger than the phenomenological ratio. The magnitude of $\mathcal{E}_3$ in our calculation is much smaller than the phenomenological value. $\mathcal{E}_2/\mathcal{E}_1$ is fixed fairly loosely in the phenomenological theory. Range parameters $\mathcal{E}_n$, calculated for CeBi and CeSb, are compared in Table IV with phenomenological parameters fitted to the magnetic properties of CeBi.[26] (The fitting of the phenomenological parameters is as described in Sec. II above.)

V. SUMMARY AND DISCUSSION

We have used a self-consistent, local-density functional, warped–muffin-tin potential to define and calculate the quantities entering the Schrieffer-Wolff version of the Anderson Hamiltonian. The non-f band states are obtained with an LMTO band structure method with Ce f states placed in corelike orbitals obtained from the resonant scattering state of a single-site Ce muffin-tin potential. The hybridization potential is taken to be the pseudopotential obtained by projecting band-f overlap out of the matrix element of a single-site Ce muffin-tin Hamiltonian between band states and the localized f state. The energies E_f and U are estimated from the eigenvalues of Ce muffin potentials derived from charge densities with 0, 1, and 2 electrons in f states.

A major approximation in the formalism we use is the identification of the difference in density functional eigenvalues with the total energy transfers appearing in the denominators of the model Hamiltonian parameters. By taking the f level to be the total energy to place an f electron at the Fermi energy, the energy difference $\varepsilon_k - E_f$ should be a good approximation to the total energy transfer for the bands that contribute most heavily to the quantities we calculate.

The formalism has been applied to the calculation of two quantities arising in the model Hamiltonian theory applied to the Ce monopnictides: the suppression in the crystal-field splitting and the range functions determining the strength of the two-ion exchange interaction. The result for the crystal-field splitting is in excellent agreement with observed values; agreement between calculated and phenomenological range parameters is fair. In assessing the significance of the relatively poorer agreement for the range parameters, it should be remembered that the result for the crystal-field dressing is exactly a calculation of a particular term arising in the Schrieffer-Wolff perturbation expansion of the Anderson Hamiltonian, and the results of our calculation may be compared directly to experiment. The calculated range parameters, however, are being compared with fitted range parameters arising from a formalism which is itself an approximation to the model Hamiltonian (this has been discussed in Sec. IV B above), and so the connection is less clear. We are pleased that the trends in the calculated range functions agree with those found in the phenomenological theory. The relation between the magnetic properties of these materials and the range parameters is rather complex, and the accuracy of the calculated range parameters can ultimately only be judged by expanding the phenomenological calculation to include all the transition channels of the range function matrix. This task is in progress. We should note, however, that as discussed below, an improved calculation will include effects of the band-f hybridization on the way in which the band structure evolves in its self-consistent determination, i.e., it will include nonlinear effects, and we expect these nonlinear effects to be more important in treating magnetic ordering than in treating crystal-field dressing for a paramagnetic system. Also the departure of the hybridization potential from spherical symmetry is apt to be more important for the magnetically ordered state.

Three factors determine the sensitivity of the present calculations: the accuracy of the self-consistent potential, the size of the mesh providing the eigenvalues and vectors for the analysis, and the energies E_f and E_f+U with respect to the Fermi energy. The potential is taken to self-consistency on a mesh of 60 special points in the irreducible wedge of the Brillouin zone. Comparison with a 240-point tetrahedral mesh suggests that the potential and

total energy are converged to within ~ 0.3 mRy. The bands used to evaluate the crystal-field suppression and the range functions are calculated on an 89-point tetrahedral mesh. Comparison with a 240-point mesh calculation for CeSb suggests that the calculation of the crystal-field suppression is converged to within about 5%. The calculation of the range functions, fourth order in the band-f interaction, is inherently more sensitive, and the convergence of the calculation is poorer. Proper convergence of a second-order perturbation calculation may require in excess of 1000 points.[28]

The calculations are somewhat sensitive to the energies E_f and U. We have used a value of $E_f - E_f = 2$ eV in our calculations. Varying this value between 1.5 and 2.5 eV produces changes in the calculated results on the order of 5%. Taking $E_F - E_f$ to be ~ 0.5 eV produces changes in the results of $\sim 30\%$ in the calculated shift in the crystal-field levels.

The calculations presented in this paper provide the initial step in the prediction of model Hamiltonian parameters from first principles. Improved calculations will include both the effects of the full anisotropy of the potential within the muffin-tin spheres and the nonlinear hybridization effects associated with the self-consistent determination of both the band states and the f states in the presence of the band-f interaction. The latter effects will occur when the bands and the f states are no longer obtained from a calculation which neglects band-f hybridization, i.e., from a calculation which is linear in hybridization, as is done presently. Including such hybridization effects will change the occupation of the band states and f states near the Fermi energy, and this will in turn alter the hybridization itself, thereby introducing nonlinear hybridization effects. The first extension of the present calculations including these improvements will be to determine the crystal-field levels of Ce compounds as a function of temperature, i.e., as a function of thermal occupation of the levels. Subsequently, we plan to introduce the nonlinear hybridization effects and the lowered symmetry of the mixing potential within the spheres into our calculations for the magnetically-ordered state.

Our purpose in this paper has not been to exhibit calculations of particular physical quantities with ultimate accuracy, but rather to investigate the utility and accuracy of the formalism as a means of predicting the parameters of the model Hamiltonian for application to understanding and predicting effects in different systems. The results presented in this paper for the Ce monopnictides would seem to suggest that this approach has the potential of providing a useful analysis for weakly hybridizing f-electron systems. A question of broader interest than the application to the weakly hybridizing cerium monopnictide systems discussed here is the possible application to more strongly hybridizing systems, in which category, for example, heavy fermion systems probably fall. It may be that including the nonlinear hybridization effects and the lowered symmetry of the mixing potential will provide sufficient improvement to treat magnetically-ordered heavy fermion systems. We have begun calculations for CeTe, and the predicted change in behavior from CeSb by adding an additional pnictogen p electron may provide a test of our ability to deal with more strongly hybridizing systems. However, it should be recognized that what is described in this paper is really a technique for calculating the various pieces needed to put a model Hamiltonian treatment of observed experimental phenomena on an absolute basis. Our present comparison to the experimental phenomenology is based on the use of the Schrieffer-Wolff (Coqblin-Schrieffer) treatment of the Anderson Hamiltonian. This limits us in principle to treating weak hybridization. However, the same technique for calculating the "pieces" (hybridization potential matrix elements, band energies, f-state energies including correlation) can be used to put any more general treatment of the Anderson Hamiltonian on an absolute basis.

ACKNOWLEDGMENT

This research was supported through the National Science Foundation under Grant No. DMR-85-04449.

APPENDIX: FOURTH-ORDER TERMS IN THE LATTICE SCHRIEFFER-WOLFF TRANSFORMATION

In this appendix we give a brief derivation of Eq. (2.7), exhibiting the cancellation of the singular terms in the exchange coupling derived with second order perturbation theory [Eq. (2.5)]. The treatment of the Schrieffer-Wolff transformation given here parallels that given in Ref. 4, but our notation is somewhat different.

The generator of the Schrieffer-Wolff transformation may be written as

$$\mathcal{S} = i \int_{-\infty}^{0} dt\, \mathcal{H}_1(t) , \tag{A1}$$

where $\mathcal{H}_1(t)$ is the band-f hybridization term in the Anderson Hamiltonian in the interaction picture. If $\mathcal{P}_n(m)$ is the projection operator for n f-electron states in the space spanned by $\{m' : m' \neq m\}$ and $\mathcal{P}_n(m,m')$ projects out n f-electron states in the space spanned by $\{m'' : m'' \neq m, m'\}$, etc., $\mathcal{H}_1(t)$ is given by

$$\mathcal{H}_1(t) \equiv e^{-i\mathcal{H}_0 t} \mathcal{H}_1 e^{-i\mathcal{H}_0 t} = \sum_{R,m,n,k} \{ V_{km}(R) c_k^{\dagger} c_m(R) \mathcal{P}_n(m;R) \exp[i(\varepsilon_k - E_f - nU)t] + \text{H.c.} \} . \tag{A2}$$

The fourth-order term in the transformed Hamiltonian is

$$\mathcal{H}^{(4)} = \tfrac{1}{8} [\mathcal{S}, [\mathcal{S}, [\mathcal{S}, \mathcal{H}_1]]] . \tag{A3}$$

We are concerned with the subset of terms in $\mathcal{H}^{(4)}$ having the form of Eq. (2.4). Carrying out the commutators in Eq. (A2), we find two terms with this form. After taking the expectation value of $\mathcal{H}^{(4)}$ in the band ground state, the first

term is

$$\mathcal{H}_1^{(4)} \equiv \tfrac{1}{8} \sum_{R_1,R_2}' \sum_{m_1,m_1'}' \sum_{m_2,m_2'}' \sum_{n_1,n_2} \sum_{k} \sum_{k'>k_F} V_{k'm_1'} V^*_{k'm_2} V_{km_2'} V^*_{km_1} e^{-i(\mathbf{k}-\mathbf{k}')\cdot(\mathbf{R}_2-\mathbf{R}_1)} c^\dagger_{m_2}(R_2) c_{m_2'}(R_2) c^\dagger_{m_1}(R_1) c_{m_1'}(R_1)$$
$$\times [\mathcal{P}_{n_2}(m_2,m_2';R_2) - \mathcal{P}_{n_2-1}(m_2,m_2';R_2)][\mathcal{P}_{n_1}(m_1,m_1';R_1) - \mathcal{P}_{n_1-1}(m_1,m_1';R_1)]$$
$$\times \left[-\frac{2}{\varepsilon-\varepsilon'} \left[\frac{1}{\varepsilon'-E_{n_1}} + \frac{1}{\varepsilon-E_{n_1}} \right] \left[\frac{1}{\varepsilon-E_{n_2}} + \frac{1}{\varepsilon'-E_{n_2}} \right] + \frac{8}{(\varepsilon-\varepsilon')(\varepsilon'-E_{n_1})(\varepsilon'-E_{n_2})} \right], \tag{A4}$$

where ε is a band energy and $E_n \equiv E_f + nU$. When $k < k_F$ in Eq. (A4), the first term in braces on the right side is the negative of the contribution resulting from treating the second-order exchange Hamiltonian [$\mathcal{H}_{\text{ex}}$ in Eq. (2.2)] with second-order perturbation theory. When $k > k_F$, this term, antisymmetric in ε and ε', vanishes. Hence the residual contribution to the exchange interaction from the sum of Eq. (A4) and $(\mathcal{H}_{\text{ex}})^2$ is the second term in braces in Eq. (A4). This term is finite, and the only fourth-order term to contribute, when $n_1 = n_2 = 0$; thus, in the limit $U \to \infty$, the total exchange interaction is given by this term. Within an f^1 basis (initial and final states with one f-electron per Ce site), n_1 and n_2 may be zero or one, and a complete description of the two-ion exchange interaction through fourth order in $\mathcal{H}_1$ requires keeping terms through first order in $1/U$.

The second term arising in the fourth-order term of the Schrieffer-Wolff transformation is

$$\mathcal{H}_2^{(4)} \equiv \frac{1}{8} \sum_{R_1,R_2}' \sum_{m_1,m_1'}' \sum_{m_2,m_2'}' \sum_{n_1,n_2} \sum_{k} \sum_{k'} V_{k'm_1'} V^*_{k'm_2} V_{km_2'} V^*_{km_1} e^{-i(\mathbf{k}-\mathbf{k}')\cdot(\mathbf{R}_2-\mathbf{R}_1)} c^\dagger_{m_2}(R_2) c_{m_2'}(R_2) c^\dagger_{m_1}(R_1) c_{m_1'}(R_1)$$
$$\times [\mathcal{P}_{n_2}(m_2,m_2';R_2) - \mathcal{P}_{n_2-1}(m_2,m_2';R_2)] \mathcal{P}_{n_1-1}(m_1,m_1';R_1)$$
$$\times \left[\frac{1}{(\varepsilon'-E_{n_1})(\varepsilon-E_{n_2})} \left[\frac{3}{\varepsilon-E_{n_1}} + \frac{1}{\varepsilon'-E_{n_2}} \right] + \frac{1}{(\varepsilon-E_{n_1})(\varepsilon'-E_{n_2})} \left[\frac{3}{\varepsilon'-E_{n_1}} + \frac{1}{\varepsilon-E_{n_2}} \right] \right]. \tag{A5}$$

With initial and final states confined to an f^1 basis set, $\mathcal{P}_n(m,m') = \delta_{n,1}$. Combining Eqs. (A4) and (A5) with the second-order perturbation term on $\mathcal{H}_{\text{ex}}$ from Eq. (2.2), and summing over allowed values of n_1 and n_2, the result is

$$\mathcal{H}^{(4)} + \sum_{i \neq 0} \langle \Phi_0 | \mathcal{H}_{\text{ex}} | \Phi_i \rangle \langle \Phi_i | \mathcal{H}_{\text{ex}} | \Phi_0 \rangle / (E_0 - E_i)$$
$$= \sum_{R_1,R_2}' \sum_{m_1,m_1'}' \sum_{m_2,m_2'}' \sum_{n_1,n_2} \sum_{k} \sum_{k'} V_{k'm_1'} V^*_{k'm_2} V_{km_2'} V^*_{km_1} e^{-i(\mathbf{k}-\mathbf{k}')\cdot(\mathbf{R}_2-\mathbf{R}_1)} c^\dagger_{m_2}(R_2) c_{m_2'}(R_2) c^\dagger_{m_1}(R_1) c_{m_1'}(R_1)$$
$$\times \left\{ \Theta(E_F-\varepsilon)\Theta(\varepsilon'-E_F) \left[\frac{1}{\varepsilon-\varepsilon'} \left[\frac{1}{\varepsilon'-E_f} - \frac{1}{\varepsilon-E_f-U} \right]^2 + \frac{2/U}{(\varepsilon-E_f-U)(\varepsilon'-E_f)} \right] \right.$$
$$+ \tfrac{1}{2}\Theta(\varepsilon-E_F)\Theta(\varepsilon'-E_F) \left[\frac{1}{(\varepsilon-E_f)(\varepsilon'-E_f)} \left[\frac{2}{U} + \frac{1}{\varepsilon-E_f} + \frac{1}{\varepsilon'-E_f} \right] \right]$$
$$+ \tfrac{1}{2}\Theta(E_F-\varepsilon)\Theta(E_F-\varepsilon') \left[\frac{1}{(\varepsilon-E_f-U)(\varepsilon'-E_f-U)} \times \left[\frac{2}{U} - \frac{1}{\varepsilon-E_f-U} - \frac{1}{\varepsilon'-E_f-U} \right] \right]$$
$$\left. - \frac{1}{4}\frac{1}{U} \left[\frac{1}{\varepsilon'-E_f-U} + \frac{1}{\varepsilon'-E_f} \right] \left[\frac{1}{\varepsilon-E_f-U} + \frac{1}{\varepsilon-E_f} \right] \right\}. \tag{A6}$$

The last term in curly brackets in Eq. (A6), the only term in which singular energy denominators remain, is recognizable as the negative of the contribution to the two-ion exchange interaction from the second-order f-banding Hamiltonian ($\mathcal{H}_b$ in Eq. (2.2)) treated in second-order perturbation theory on f states through first order in $1/U$:

$$
\begin{aligned}
&-\sum_{i\neq 0}\langle\Phi_0\,|\,\mathcal{H}_b\,|\,\Phi_i\rangle\langle\Phi_i\,|\,\mathcal{H}_b\,|\,\Phi_0\rangle/U \\
&\quad=-\sum_{R_1,R_2}{}'\sum_{m_1,m_1'}{}'\sum_{m_2,m_2'}{}'\sum_{n_1,n_2}\sum_{k,k'}\mathcal{J}(k',m_2',R_2,n_2;k',m_1,R_1,n_1)\mathcal{J}(k,m_1',R_1,n_1;k,m_2,R_2,n_2) \\
&\qquad\qquad\times c^{\dagger}_{m_2}(R_2)c_{m_2'}(R_2)c^{\dagger}_{m_1}(R_1)c_{m_1'}(R_1)\delta_{n_1 1}\delta_{n_2 0} \\
&\quad=\sum_{R_1,R_2}{}'\sum_{m_1,m_1'}{}'\sum_{m_2,m_2'}{}'\sum_{n_1,n_2}\sum_{k}\sum_{k'}V_{k'm_1'}V^{*}_{k'm_2}V_{km_2'}V^{*}_{km_1}e^{-i(\mathbf{k}-\mathbf{k}')\cdot(\mathbf{R}_2-\mathbf{R}_1)}c^{\dagger}_{m_2}(R_2)c_{m_2'}(R_2)c^{\dagger}_{m_1}(R_1)c_{m_1'}(R_1) \\
&\qquad\qquad\times\frac{1}{4}\frac{1}{U}\left[\frac{1}{\varepsilon'-E_f-U}+\frac{1}{\varepsilon'-E_f}\right]\left[\frac{1}{\varepsilon-E_f-U}+\frac{1}{\varepsilon-E_f}\right]. \qquad \text{(A7)}
\end{aligned}
$$

Hence the total two-ion exchange interaction, including all terms consistently through fourth order in $\mathcal{H}_1$, is free of the divergences occurring in second-order perturbation theory. A comparison of Eqs. (A6), (A7), (2.4), and (2.6) gives Eq. (2.7) as the proper function of energy to be used in calculating the range functions $\mathcal{E}(R)$.

[1]B. R. Cooper, R. Siemmann, D. Yang, P. Thayamballi, and A. Banerjea, in *Handbook on the Physics and Chemistry of the Actinides,* edited by A. J. Freeman and G. H. Lander (North-Holland, Amsterdam, 1985), Vol. 2, Chap. 6, pp. 435–500.

[2]R. J. Birgeneau, E. Bucher, J. P. Maita, L. Passel, and K. C. Turberfield, Phys. Rev. B **8**, 5345 (1973).

[3]B. R. Cooper, J. Less-Common Met. **133**, 31 (1987).

[4]J. R. Schrieffer and P. A. Wolff, Phys. Rev. **149**, 491 (1966).

[5]B. Cornut and B. Coqblin, Phys. Rev. B **5**, 4541 (1972). Our notation is similar to, but not identical with, the notation of Cornut and Coqblin.

[6]J. M. Wills and W. A. Harrison, Phys. Rev. B **28**, 4363 (1983).

[7]W. A. Harrison, Phys. Rev. B **28**, 550 (1983).

[8]P. Thayamballi and B. R. Cooper, Phys. Rev. B **30**, 2931 (1984).

[9]B. Coqblin and J. R. Schrieffer, Phys. Rev. **185**, 847 (1969).

[10]R. Siemman and B. R. Cooper, Phys. Rev. Lett. **44**, 1015 (1980).

[11]J. M. Wills and B. R. Cooper, J. Magn. Magn. Mater. **54-57**, 1049 (1986).

[12]H. L. Skriver, *The LMTO Method* (Springer, Berlin, 1984).

[13]L. Hedin and B. I. Lundqvist, J. Phys. C **4**, 2064 (1971).

[14]D. D. Koelling and B. N. Harmon, J. Phys. C **10**, 3107 (1977).

[15]D. J. Chadi and M. L. Cohen, Phys. Rev. B **8**, 5747 (1973).

[16]A. Messiah, *Quantum Mechanics* (Wiley, New York, 1958), Vol. 1, p. 397.

[17]M. R. Norman, D. D. Koelling, A. J. Freeman, H. J. F. Jansen, B. I. Min, T. Oguchi, and Ling Ye, Phys. Rev. Lett. **53**, 1673 (1984).

[18]J. F. Herbst, D. N. Lowy, and R. E. Watson, Phys. Rev. B **6**, 1913 (1972).

[19]G. Gilat and N. R. Bharatiya, Phys. Rev. B **12**, 3479 (1975).

[20]H. Heer, A. Furrer, W. Halg, and O. Vogt, J. Phys. C **12**, 5207 (1979).

[21]J. Callaway, *Quantum Theory of the Solid State* (Academic, New York, 1976).

[22]H. Takahashi, K. Takegahara, A. Yanase, and T. Kasuya, in *Valence Instabilities,* edited by P. Wachter and H. Boppart (North-Holland, Amsterdam, 1982), pp. 379–383.

[23]The magnetic structures are described and original references are given in Ref. 1.

[24]J. Rossat-Mignod, D. Delacote, J. M. Effantin, C. Vetteir, and O. Vogt, Physica **120B**, 163 (1983).

[25]P. Thayamballi, D. Yang, and B. R. Cooper, Phys. Rev. B **29**, 4049 (1984).

[26]P. Thayamballi and B. R. Cooper, Phys. Rev. B **31**, 5911 (1985).

[27]A. R. Edmonds, *Angular Momentum in Quantum Mechanics* (Princeton University Press, New Jersey, 1974).

[28]M. S. S. Brooks, in Proceedings of the 1985 Los Alamos Workshop on Hybridizing f-Electron Systems (unpublished).